NASA TECHNICAL NOTE

NASA TN D-4397

C.1

NASA TN D-4397

COMPARISON OF EXPERIMENTAL AND THEORETICAL SHOCK SHAPES AND PRESSURE DISTRIBUTIONS ON FLAT-FACED CYLINDERS AT MACH 10.5

by Mamoru Inouye, Joseph G. Marvin, and A. Richard Sinclair

Ames Research Center
Moffett Field, Calif.

NATIONAL AERONAUTICS AND SPACE ADMINISTRATION • WASHINGTON, D. C. • FEBRUARY 1968

COMPARISON OF EXPERIMENTAL AND THEORETICAL SHOCK SHAPES AND PRESSURE DISTRIBUTIONS ON FLAT-FACED CYLINDERS AT MACH 10.5

By Mamoru Inouye, Joseph G. Marvin,
and A. Richard Sinclair

Ames Research Center
Moffett Field, Calif.

NATIONAL AERONAUTICS AND SPACE ADMINISTRATION

For sale by the Clearinghouse for Federal Scientific and Technical Information
Springfield, Virginia 22151 – CFSTI price $3.00

COMPARISON OF EXPERIMENTAL AND THEORETICAL SHOCK SHAPES AND PRESSURE DISTRIBUTIONS ON FLAT-FACED CYLINDERS AT MACH 10.5

By Mamoru Inouye, Joseph G. Marvin,
and A. Richard Sinclair

Ames Research Center

SUMMARY

Shock-wave shapes and surface pressures were measured on flat-faced cylinders with shoulder to base radius ratios of 0.0, 0.05, 0.15, 0.25, and 0.5. The measured values were compared with one- and two-strip numerical solutions obtained by the method of integral relations. The two-strip solutions predicted adequately both the shock shapes and surface pressures. The one-strip solutions predicted adequately the shock shapes but underestimated the surface pressures.

The shock-wave standoff distances decreased linearly with increasing shoulder radius. The computed stagnation-point velocity gradients increased with increasing shoulder radius, but not linearly.

INTRODUCTION

Solutions for the inviscid shock layer flow over blunt bodies may be obtained by numerical integration of the governing differential equations (see ref. 1 for a comprehensive review). The methods employed are inverse or direct depending on how the initial conditions are specified. Notable examples of these methods may be found in references 2 and 3, respectively.

More recently, in reference 4, the inverse method was used to obtain solutions for spherical and ellipsoidal noses over a wide range of free-stream conditions. In this method the shock shape is prescribed and the flow field including body location is calculated. However, for very blunt nose shapes, particularly those with sharp corners, the method described in reference 4 fails because of numerical difficulties. To calculate the flow over bodies not amenable to solution by the inverse method, Harvard Lomax and Harry Bailey of Ames Research Center formulated and programmed a direct method of solution, commonly referred to as the method of integral relations. In this method, the shock layer is divided into strips. The variations of the flow properties across the strips are represented by polynomials. The degree of the polynomial depends on the number of strips, and the accuracy of the method increases with more strips. For practical reasons, the number of strips is limited to one or two, which makes the method approximate.

Surface pressure measurements may be used to assess the validity of approximate theoretical methods used to describe the inviscid flow over various body shapes. Shock-wave measurements serve the same purpose although they are not so definitive. Surface pressures were measured on flat-faced cylinders with different shoulder radii (ref. 5). Some comparisons were made with solutions obtained by the method of integral relations mentioned above with one strip. Subsequently, schlieren photographs of the shock configuration were taken for the same models and test conditions, and further computations of the flow field were made with two strips.

The purpose of this report is to present the measured shock wave shapes and surface pressure distributions and to compare them with predictions by the method of integral relations for one and two strips.

SYMBOLS

D	cylinder diameter
M	Mach number
N	number of strips
p	pressure
R	cylinder radius
Re	Reynolds number, $\frac{\rho_\infty V_\infty D}{\mu_\infty}$
r_s	shoulder radius
s	distance along surface measured from stagnation point
T	temperature
V	velocity
V_o	velocity midway between body and shock for $y = 0$
x,y	cylindrical coordinates with origin at stagnation point
Δ	shock standoff distance for $y = 0$
μ	viscosity
ρ	density

Subscripts

∞ free stream

st stagnation point on body

t tunnel stagnation chamber

APPARATUS AND TEST CONDITIONS

The test data were obtained in the Ames 3.5-Foot Hypersonic Wind Tunnel (refs. 6 and 7) at $M_\infty = 10.5$ with $p_t = 123$ atm and $T_t = 1160^\circ$ K. The corresponding free-stream Reynolds number, based on model diameter, was 1.2×10^6.

The model configuration (fig. 1) consisted of a flat-faced cylinder with a shoulder radius joining the flat nose and cylindrical afterbody. The cylindrical afterbody radius was 8.89 cm. Ratios of shoulder radius to body radius (r_s/R) were 0.0, 0.05, 0.15, 0.25, and 0.5.

Schlieren photographs of the models were obtained with a 70-mm shutter camera and a conventional two-mirror schlieren system with a single pass continuous light source. Measurements of the shock-wave shapes were made directly from 8×7.5 inch prints of the 70-mm film with an indexing oscillograph trace reader equipped with a digitized output. All measurements were accurate to ± 0.005 inch.

The pressures were measured with strain-gage transducers (pressure range from 0 to 0.3 atm) and recorded on magnetic tape. The maximum error was estimated to be ± 1 percent of the measured pressure. The pressure models were inserted in the air stream after steady flow was established in the test section. Further details regarding the pressure model construction and test techniques are given in reference 5.

DISCUSSION OF ANALYTICAL METHOD

The mathematical formulation of the method of integral relations will not be presented here. Instead, the following paragraphs will describe the limitations inherent in the present method and the iteration of initial conditions required for one- and two-strip solutions. (The method is not truly direct.)

A limitation of the present method is that it does not permit integration beyond the sonic point on the body, and for two-strip solutions, may terminate earlier. The latter situation arises when the tangential component (tangent to body) of velocity midway between the body and shock approaches the local sonic speed. This will be shown to occur for $r_s/R = 0.5$ and for a sphere.

Another limitation is that the entropy at the body surface is not required to be constant. Consequently, where the flow becomes sonic (M = 1) p/p_{st} may not necessarily correspond to the isentropic flow value. The error is naturally less for the two strip solution.

Initial conditions along the stagnation streamline are required to begin the present method. Certain of these conditions may be calculated readily for a blunt-nosed body, and one initial condition per strip must be iterated. The flow properties just behind the normal shock satisfy the Rankine-Hugoniot relations and those at the body surface are the result of a subsequent isentropic compression to stagnation conditions. For the conditions of the present tests the gas can be considered thermally perfect air with the thermodynamic properties tabulated in reference 8.

In order to obtain a one-strip solution for a given body shape, the shock standoff distance, Δ, must be iterated as follows. With a sharp corner, an arbitrary value of Δ is selected, and the location of the sonic point determines R (no iteration is necessary). With a rounded shoulder, as Δ is increased, the sonic point moves off the flat face and retrogresses along the rounded shoulder. Too large a value of Δ prevents the surface Mach number from reaching unity. Thus, there is a range of values of Δ that yields solutions corresponding to various body profiles beyond the sonic point. The present method is unable to distinguish the solution corresponding to a particular profile because it cannot proceed into the transonic region on the surface that still has influence in the subsonic region. The solutions presented in this report were selected so that Δ decreases monotonically with increasing r_s/R. For a sphere, the flow field is such that this ambiguity does not occur, and Δ is iterated to determine the largest value that results in the surface Mach number reaching unity.

In order to obtain a two-strip solution, the velocity, V_o, at the midpoint of the stagnation streamline must be iterated as well as Δ. For a given value of Δ, too large a value of V_o results in a shock wave that does not decay monotonically away from the axis, and too small a value results in the surface Mach number never reaching unity. There exists a set of values of Δ and V_o which produce apparently satisfactory solutions. Some judgment must be exercised in determining the best one, and those reported here are not necessarily optimized with respect to the assumed values of Δ and V_o.

RESULTS AND DISCUSSION

Shock Wave Shape

The general character of the flow field ahead of the flat-faced cylinder may be observed in the schlieren photographs presented in figure 2 for r_s/R = 0.0, 0.05, 0.15, 0.25, 0.50. Even with a flat face, the shock wave retains an elliptical shape.

The quantitative effects of the shoulder radius may be obtained from figure 3 where all the shocks have been superimposed. The curves represent

fairings through points measured from both the upper and lower halves of the schlieren photographs. As r_s/R is increased, the shock wave is displaced inward, and its radius of curvature is decreased.

The shock-wave shapes calculated by the present method of integral relations are shown in figure 4 for $0 \leq r_s/R \leq 1.0$. The initial values of Δ and V_o are indicated in the figure. The one- and two-strip solutions are not markedly different except in the transonic region. For $r_s/R = 0.5$ and a sphere, the two-strip solution terminates much closer to the axis than the one-strip solution as a result of the sonic condition on the midstrip noted in the previous section. For the smaller shoulder radii, the differences in the end points of the shock wave are the result of differences in the location of the sonic point on the body.

The shock-wave coordinates measured from the schlieren pictures for $0 \leq r_s/R \leq 0.5$ are also shown in figures 4(a) to 4(e) for comparison. The two-strip solutions agree well with the experimental results. The one-strip solutions also agree well except for small values of the shoulder radius and in the transonic region.

No schlieren photographs were taken for a sphere, but the shock shape used in the inverse method of reference 4 is shown in figure 4(f) for comparison. The two-strip solution is indistinguishable from the inverse solution for $y/R \leq 0.5$. The one-strip solution deviates in the transonic region.

Shock-Wave Standoff Distance

The shock-wave standoff distance, Δ/R, is shown in figure 5 as a function of r_s/R. Symbols are plotted for the values measured from the schlieren photographs, the one- and two-strip solutions, and the inverse solution for a sphere. For $r_s/R \leq 0.5$, Δ decreases linearly with r_s/R, consistent with the results of reference 9. For the smallest shoulder radii, the values from the one- and two-strip solutions are less than the measured values, with the two-strip solution showing better agreement. For larger shoulder radii, all of the measurements and predictions agree well.

Surface Pressure Distributions

The surface pressure distributions calculated by the present method are shown in figure 6 for $0 \leq r_s/R \leq 1.0$. In general, the two-strip solution predicts a higher pressure over the surface than the one-strip solution; these differences are much larger than those shown previously for the shock-wave shape. For $r_s/R = 0$, the pressure remains within 10 percent of the stagnation point value over three-fourths of the surface and then decreases rapidly toward the sonic value at the corner. As r_s/R is increased, the surface pressure begins to drop off closer to the axis, and for a sphere, it has a variation similar to the cosine function. For the latter case, the one-strip solution for the pressure distribution is extremely sensitive to the initial

value of Δ. An increase of 1 percent in Δ leads to an order of magnitude larger change in the surface pressure in the transonic region. In order to obtain the solution for a spherical nose, Δ must be specified to an absurd and unnecessary accuracy.

The surface pressure measurements for $0.05 \leq r_s/R \leq 0.50$ are shown in figures 6(b) to 6(e) for comparison. The slight asymmetry of the pressure distributions is due to small angles of attack. The two-strip solutions agree well with the experimental results; the one-strip solutions predict lower pressures.

The pressure distribution for a sphere from the inverse method of reference 4 is shown in figure 6(f). The two-strip solution is indistinguishable from the inverse solution for $s/R \leq 0.35$, at which point the pressure deviates because of the limited accuracy of Δ and V_o. Also shown in the figure are surface pressures measured by Cleary (ref. 10) and Rakich and Menees (ref. 11) on hemispheres tested in the same wind tunnel used to obtain the present results. The experimental results agree well with the two-strip and inverse solutions.

Stagnation-Point Velocity Gradient

The velocity gradient along the surface at the stagnation point is required for heat-transfer calculations. Newtonian theory is commonly used for spherical noses, but it is not applicable to flat-faced bodies for which it would predict a zero velocity gradient.

The stagnation-point velocity gradients calculated by the present method are shown in figure 7. The effect of increasing the shoulder radius is to increase the velocity gradient, the increase being small for small shoulder radii but becoming quite large for a sphere. Consistent with the pressure distributions shown in figure 6, the two-strip solution predicts a smaller velocity gradient than the one-strip solution; for example, 25 to 30 percent less for $r_s/R \leq 0.50$. For a sphere, the difference is 15 percent. The velocity gradient from the inverse solution (ref. 4) agrees with the result from the two-strip solution.

The surface pressure measurements are not sufficiently accurate to obtain a velocity gradient. However, the stagnation-point heat-transfer measurements from reference 5 may be used to deduce the velocity gradients. As shown in figure 7, these values correlate with the one-strip solutions. Also shown are the results of Zoby and Sullivan (ref. 12) obtained from a correlation of experimental pressure distributions for a range of Mach numbers above 4.0. These results for $0 \leq r_s/R \leq 0.3$ lie between the one- and two-strip solutions. For a sphere, their result is the value for Newtonian flow and is about 5 percent lower than the two-strip and inverse solutions. Since the stagnation-point heating rate varies as the square root of velocity gradient, either the one- or two-strip solution will give reasonably accurate estimates of heat transfer.

CONCLUSIONS

Comparisons of experimental shock shapes and surface pressures on flat-faced cylinders with theoretical solutions obtained by the method of integral relations resulted in the following conclusions:

1. The shock shapes are adequately predicted by both the one- and two-strip solutions.

2. The shock standoff distance decreases linearly with increasing shoulder radius.

3. The surface pressures are adequately predicted by the two-strip solutions but underestimated by the one-strip solutions.

4. The stagnation-point velocity gradients from the two-strip solutions are 15 ($r_s/R = 1$) to 30 percent ($r_s/R = 0$) lower than the gradients from the one-strip solutions. Either solution is adequate for estimating stagnation-point heating rates.

Ames Research Center
National Aeronautics and Space Administration
Moffett Field, Calif., 94035, Nov. 3, 1967
129-01-09-01-00-21

REFERENCES

1. Hayes, Wallace D.; and Probstein, Ronald F.: Hypersonic Flow Theory, Second ed. Vol. 1 of Inviscid Flows. Academic Press, N. Y., 1966.

2. Van Dyke, Milton D.: The Supersonic Blunt-Body Problem - Review and Extension. J. Aerospace Sci., vol. 25, no. 8, Aug. 1958, pp. 485-496.

3. Belotserkovskii, O. M.: The Calculation of Flow Over Axisymmetric Bodies With a Detached Shock Wave. Computation Center, Acad. Sci., Moscow, USSR, 1961. Translated and edited by Springfield, J. F.: RAD-TM-62-64, AVCO Corp., 1962.

4. Lomax, Harvard; and Inouye, Mamoru: Numerical Analysis of Flow Properties About Blunt Bodies Moving at Supersonic Speeds in an Equilibrium Gas. NASA TR R-204, 1964.

5. Marvin, Joseph G.; and Sinclair, A. Richard: Convective Heating in Regions of Large Favorable Pressure Gradient. AIAA J., vol. 5, no. 11, Nov. 1967, pp. 1940-1948.

6. Holdaway, George H.; Polek, Thomas E.; and Kemp, Joseph H., Jr.: Aerodynamic Characteristics of a Blunt Half-Cone Entry Configuration at Mach Numbers of 5.2, 7.4, and 10.4. NASA TM X-782, 1963.

7. Polek, Thomas E.; Holdaway, George H.; and Kemp, Joseph H., Jr.: Flow Field and Surface Pressures on a Blunt Half-Cone Entry Configuration at Mach Numbers of 7.4 and 10.4. NASA TM X-1014, 1964.

8. Hilsenrath, Joseph, et al.: Tables of Thermodynamic and Transport Properties of Air, Argon, Carbon Dioxide, Carbon Monoxide, Hydrogen, Nitrogen, Oxygen, and Steam. Cir. 564, U.S. National Bureau of Standards, Nov. 1, 1955.

9. Stollery, J. L.; and Maull, D. J.: A Note on Shock Detachment Distance. J. Roy. Aero. Soc., vol. 64, no. 594, June 1960, pp. 357-359.

10. Cleary, Joseph W.: An Experimental and Theoretical Investigation of the Pressure Distribution and Flow Fields of Blunted Cones at Hypersonic Mach Numbers. NASA TN D-2969, 1965.

11. Rakich, John V.; and Menees, Gene P.: A Theoretical and Experimental Study of Hypersonic Flow Over Flared Bodies at Incidence. NASA TN D-3218, 1966.

12. Zoby, Ernest V.; and Sullivan, Edward M.: Effects of Corner Radius on Stagnation-Point Velocity Gradients on Blunt Axisymmetric Bodies. NASA TM X-1067, 1965.

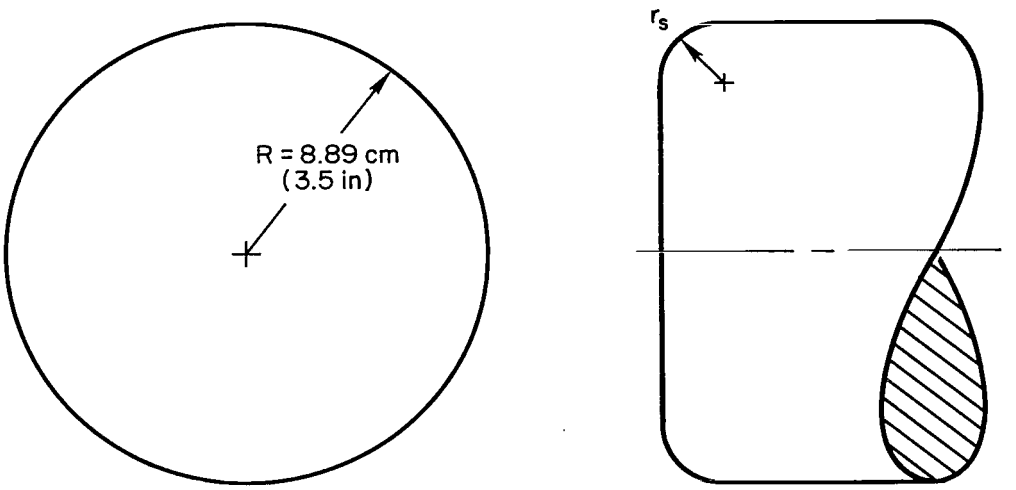

Fig. 1.- Flat-faced cylinder models.

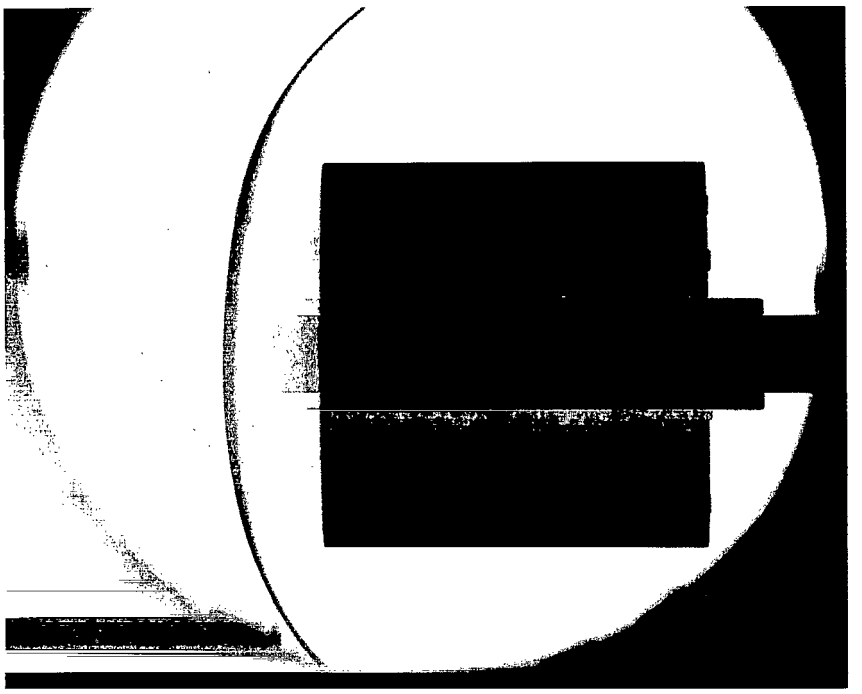

(a) $r_s/R = 0.0$

Fig. 2.- Schlieren photographs of test models for various ratios of r_s/R; $M_\infty = 10.5$, $\alpha = 0^\circ$.

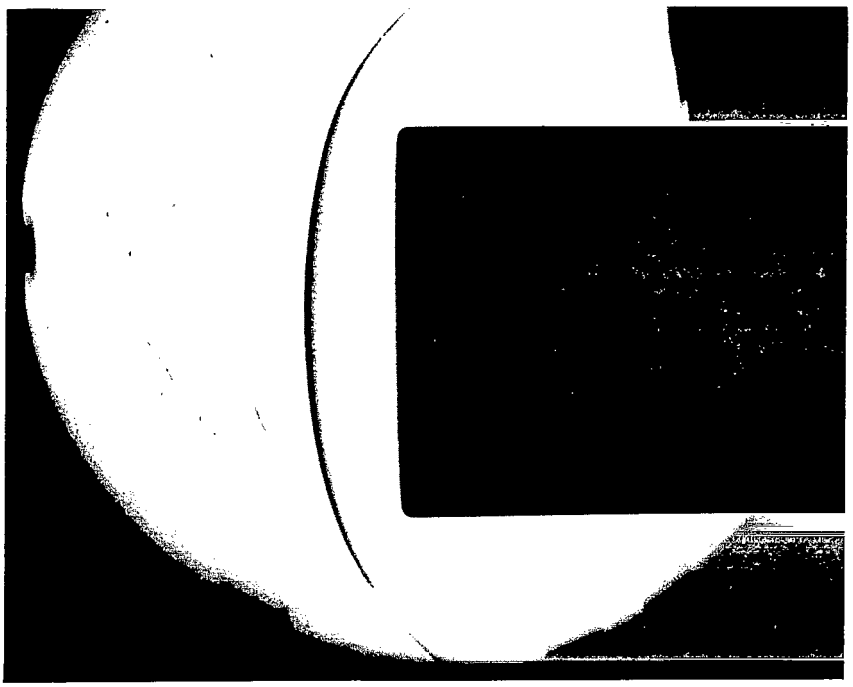

(b) $r_s/R = 0.05$

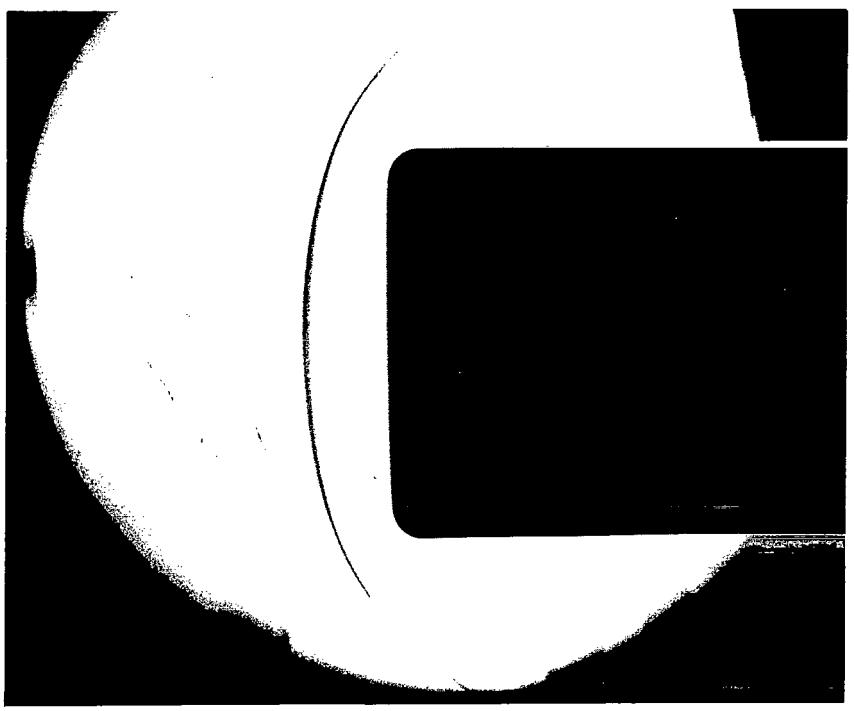

(c) $r_s/R = 0.15$

Fig. 2.- Continued.

(d) $r_s/R = 0.25$

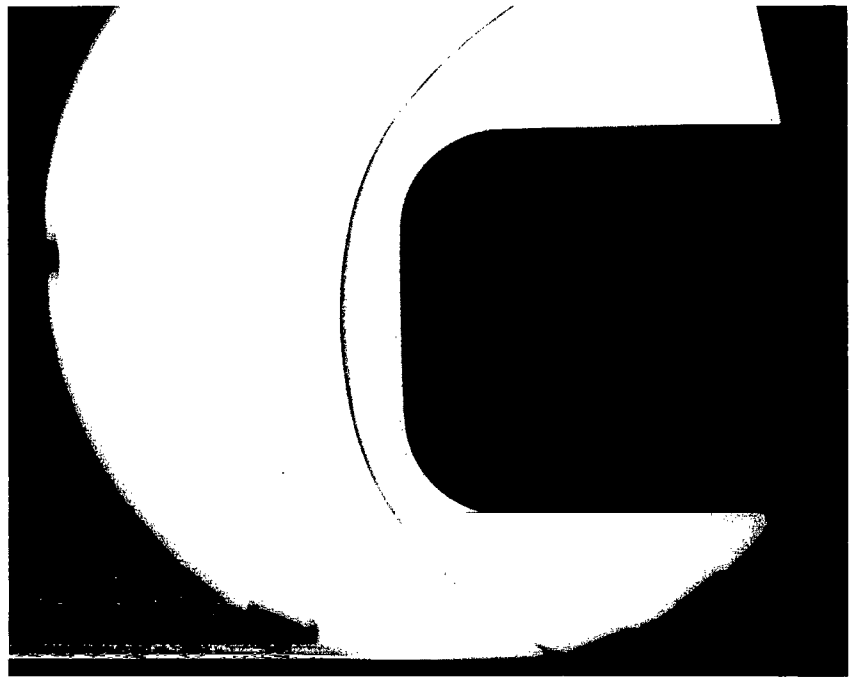

(e) $r_s/R = 0.50$

Fig. 2.- Concluded.

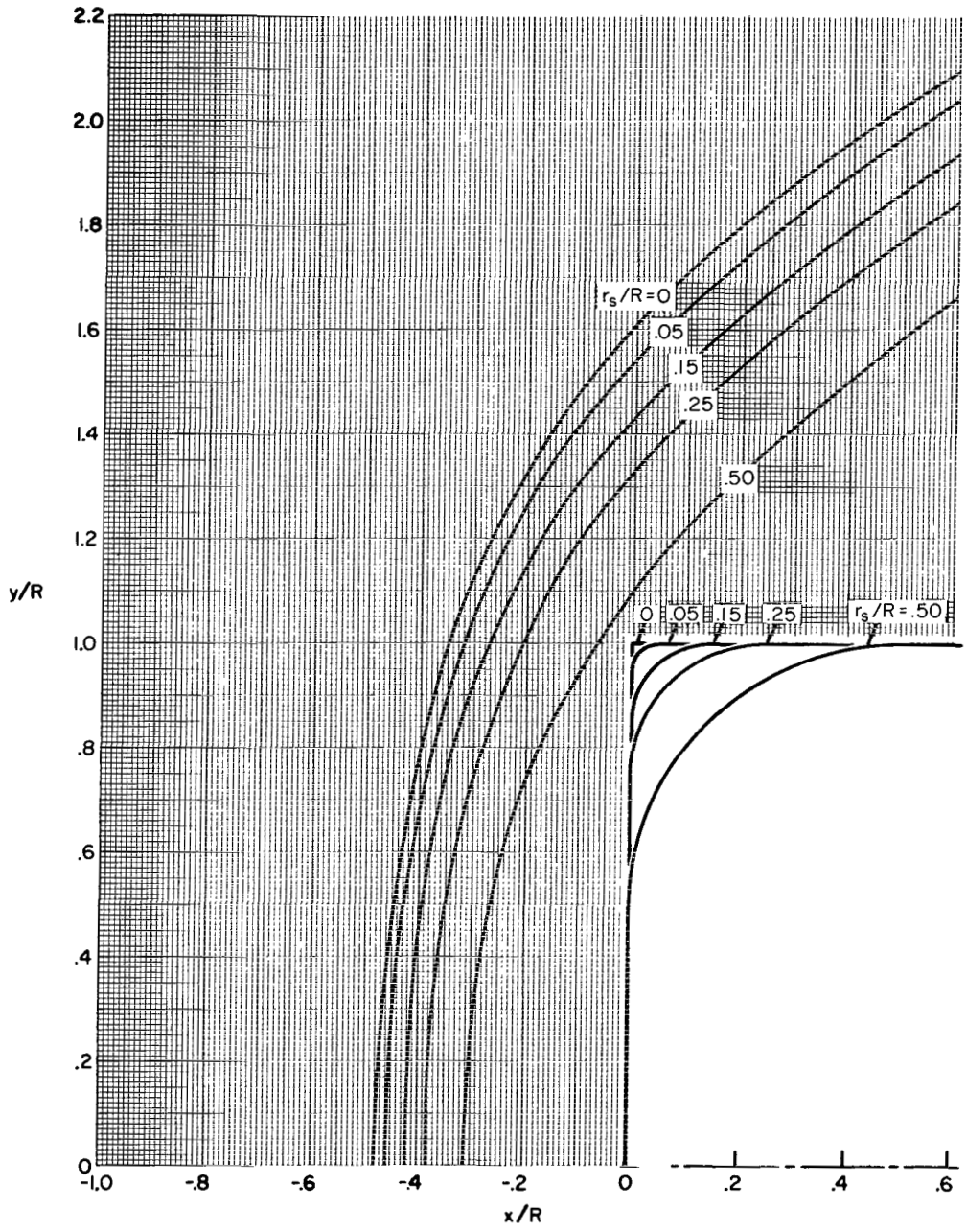

Fig. 3.- The influence of shoulder radius on shock wave shapes and positions; $M_\infty = 10.5$.

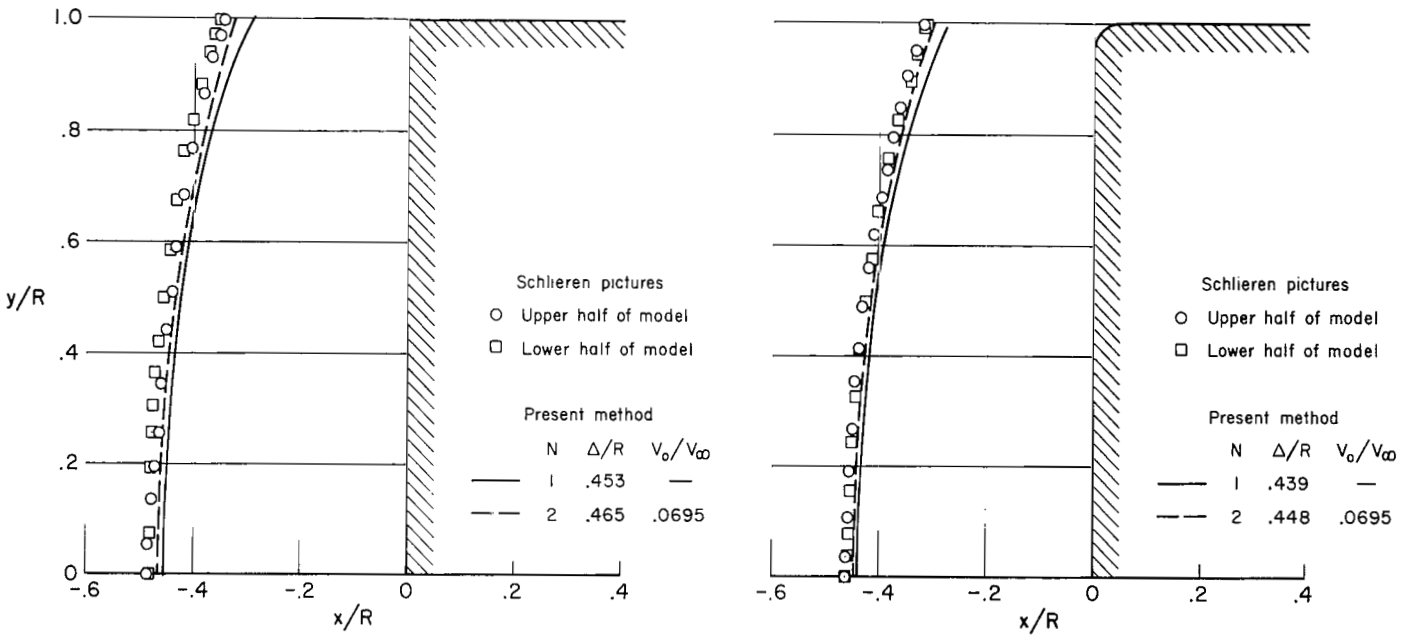

(a) $r_s/R = 0$

(b) $r_s/R = 0.05$

Fig. 4.- Shock shape for flat-faced cylinder with rounded shoulders; $M_\infty = 10.5$.

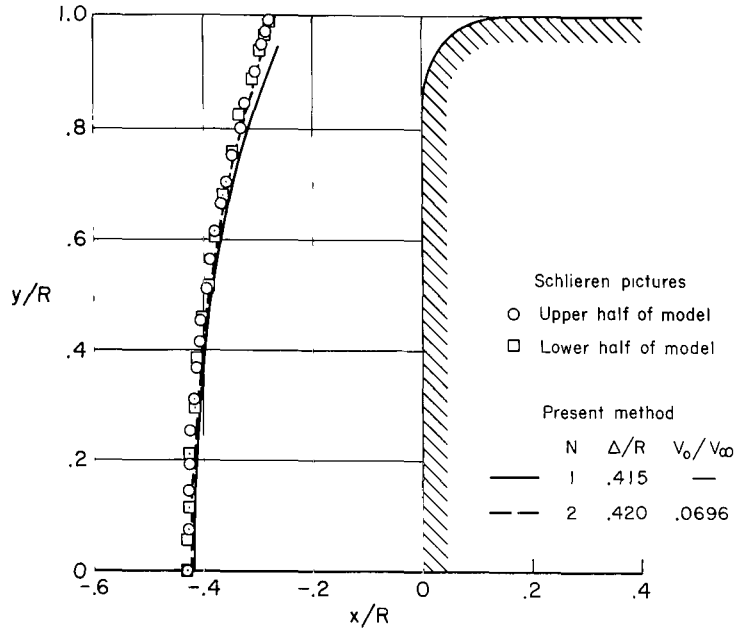

(c) $r_s/R = 0.15$

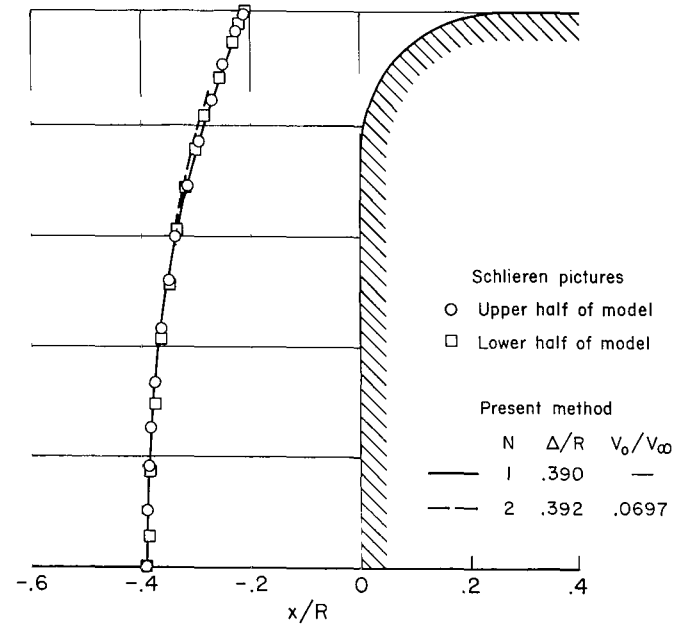

(d) $r_s/R = 0.25$

Fig. 4.- Continued.

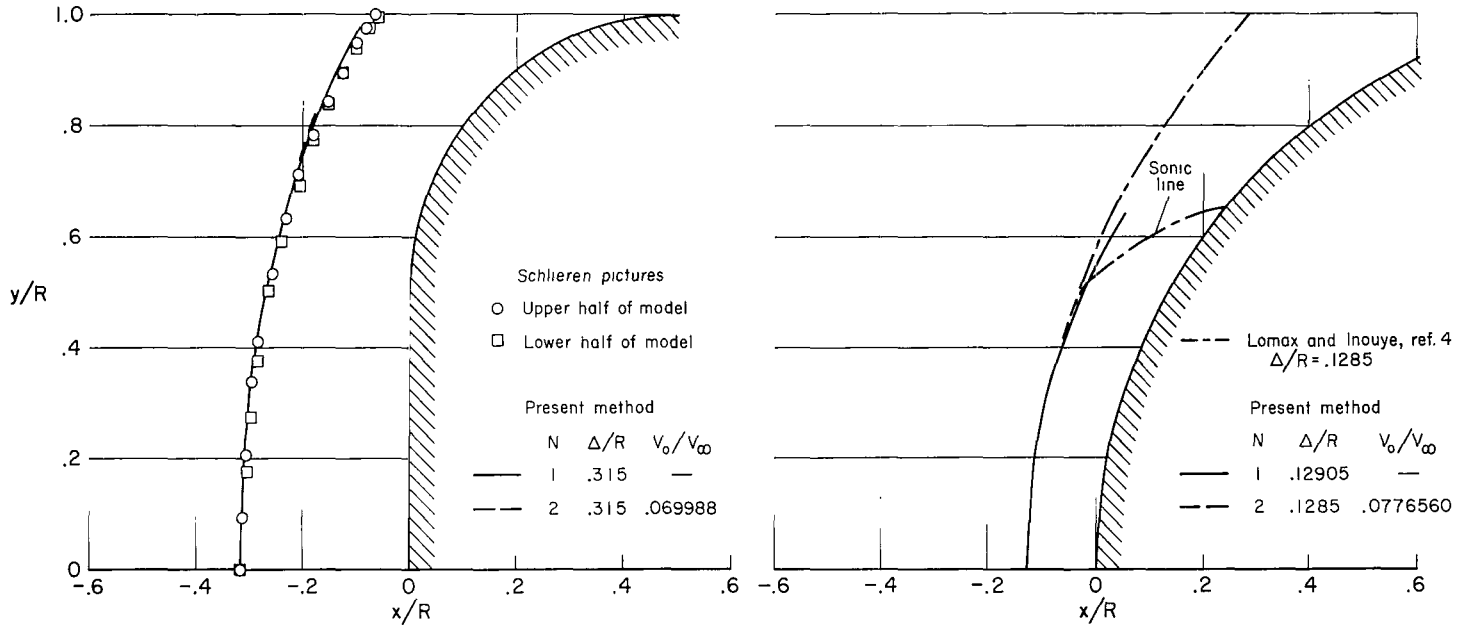

(e) $r_s/R = 0.50$

(f) $r_s/R = 1.0$

Fig. 4.- Concluded.

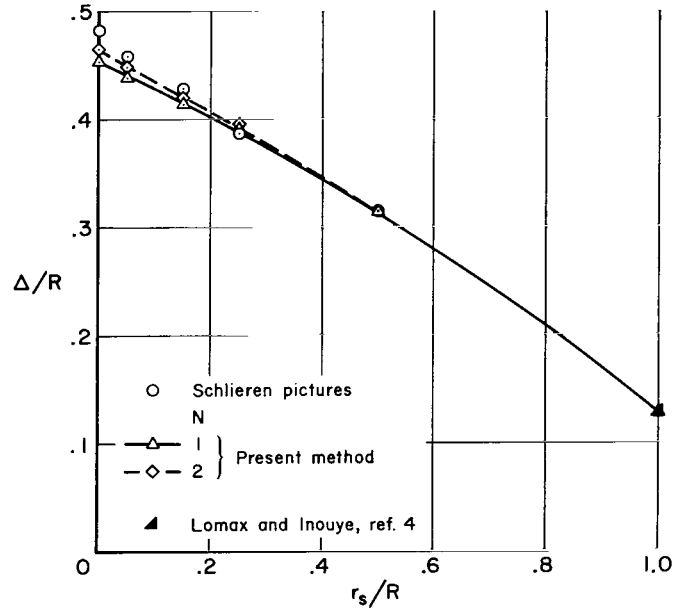

Fig. 5.- Shock standoff distance for flat-faced cylinder with rounded shoulders; $M_\infty = 10.5$.

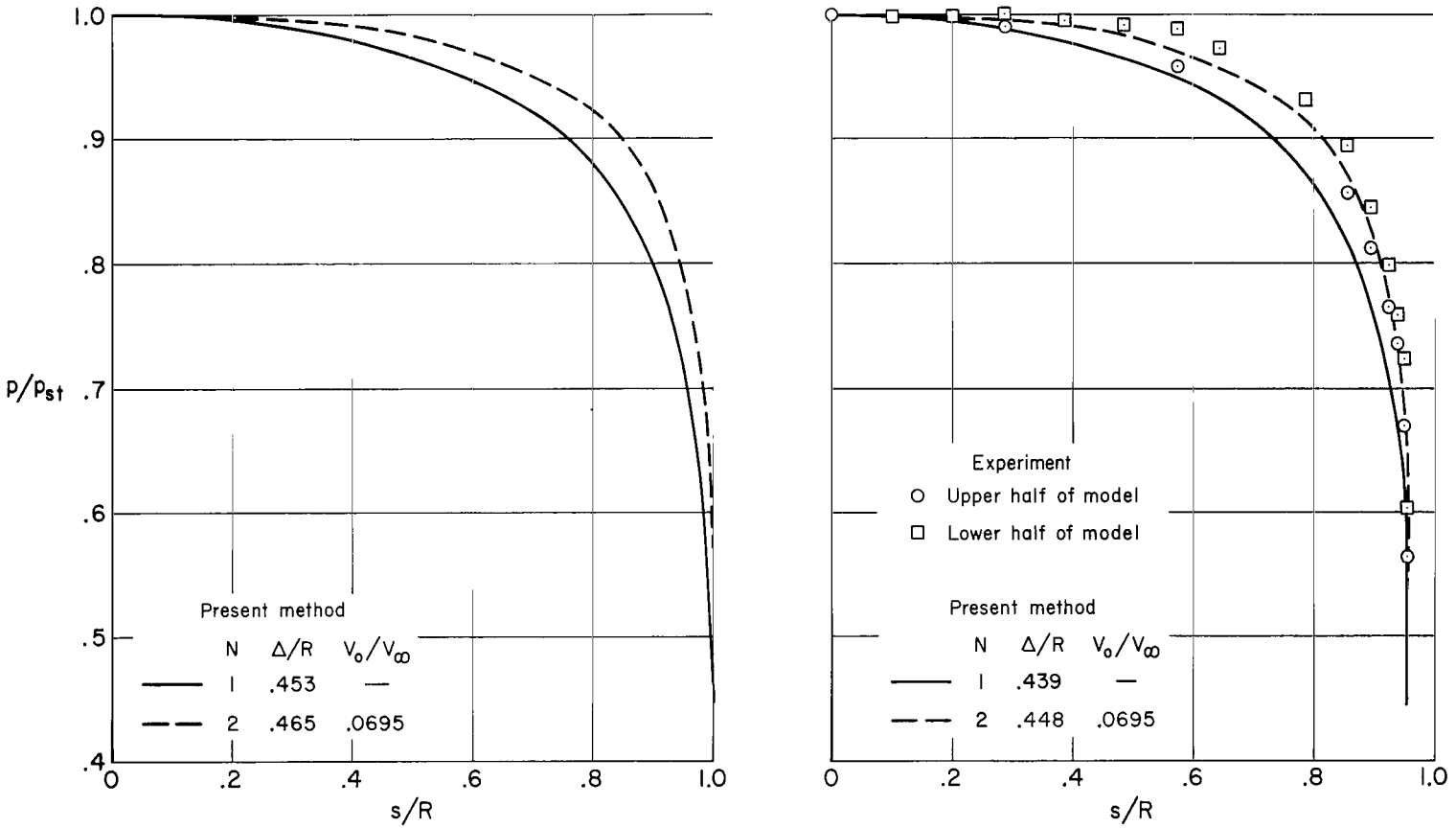

(a) $r_s/R = 0$

(b) $r_s/R = 0.05$

Fig. 6.- Pressure distribution on flat-faced cylinder with rounded shoulders; $M_\infty = 10.5$.

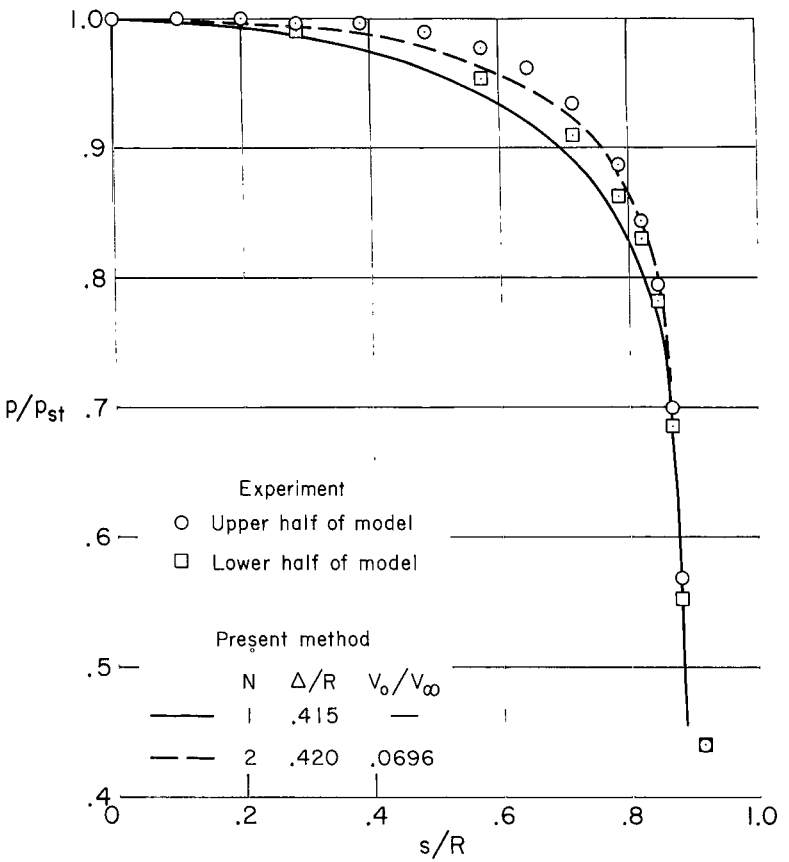

(c) $r_s/R = 0.15$

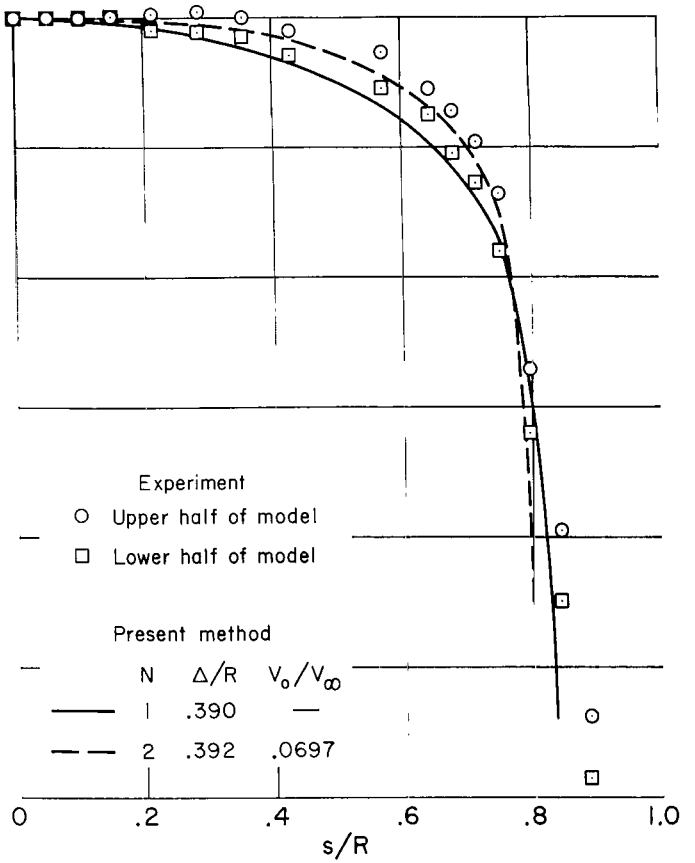

(d) $r_s/R = 0.25$

Fig. 6.- Continued.

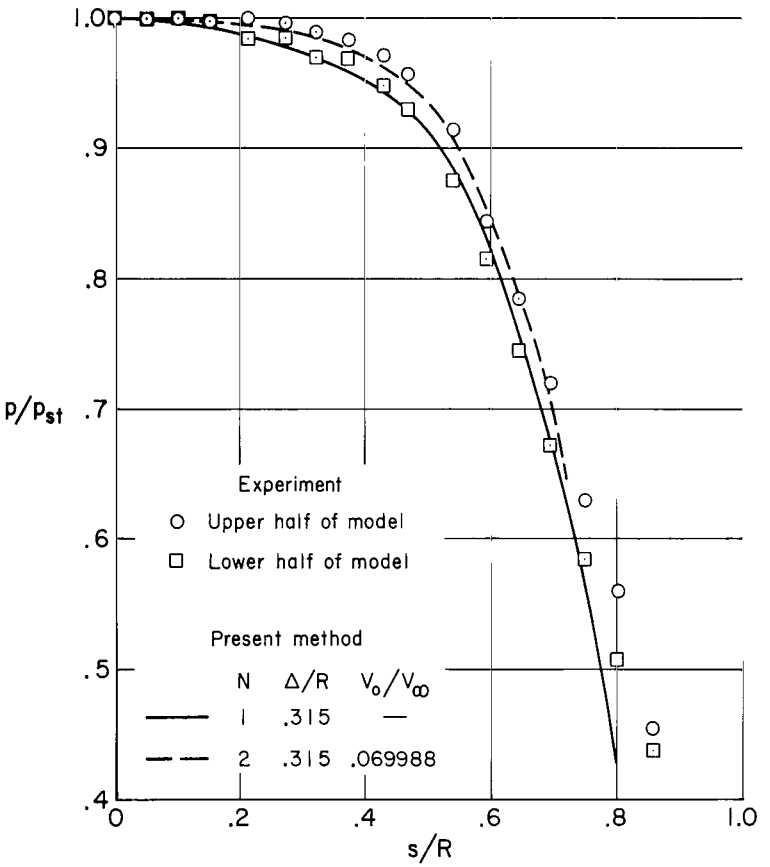

(e) $r_s/R = 0.50$

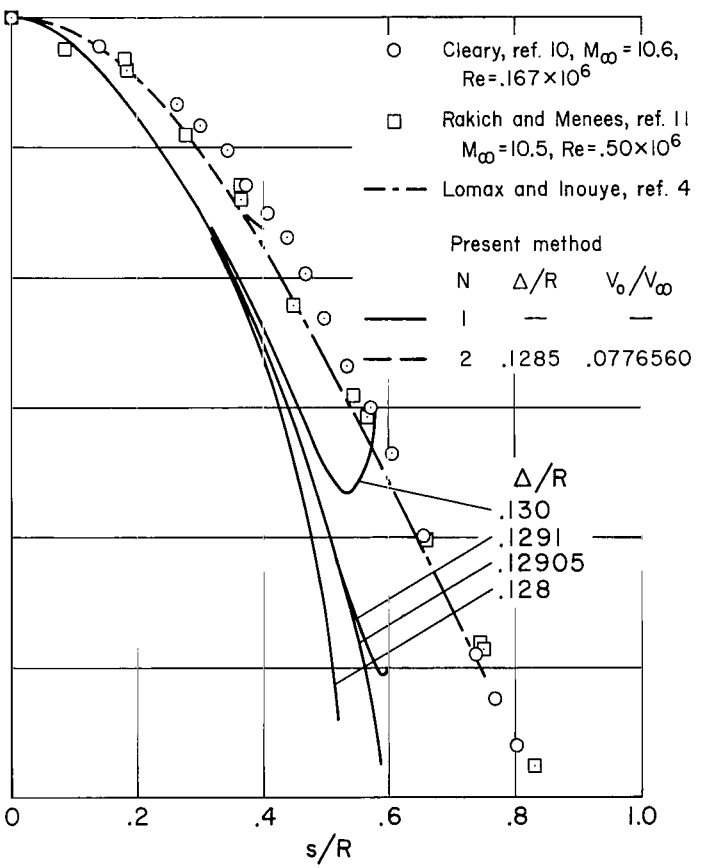

(f) $r_s/R = 1.0$

Fig. 6.- Concluded.

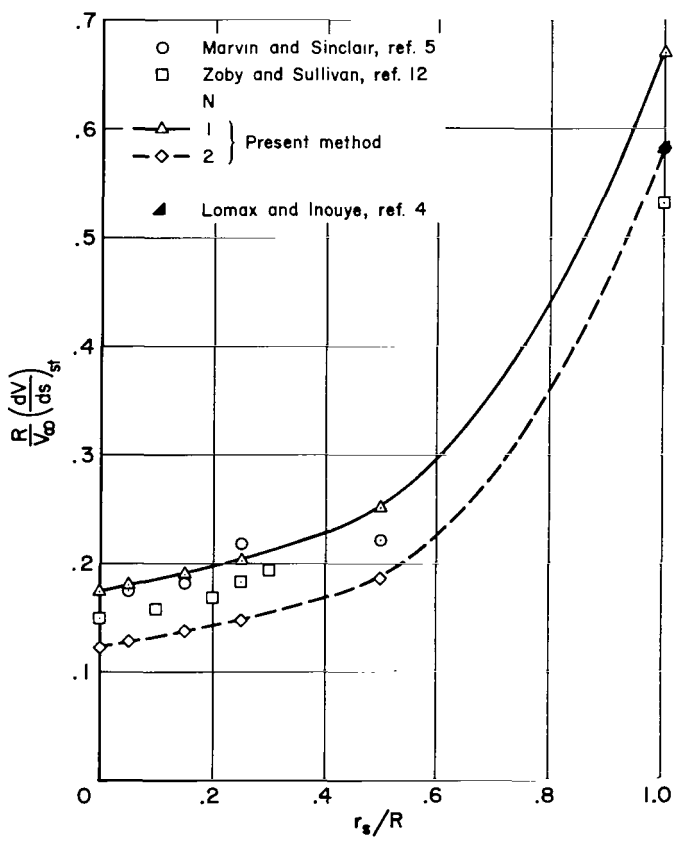

Fig. 7.- Stagnation-point velocity gradient on flat-faced cylinder with rounded shoulders; $M_\infty = 10.5$.

NASA-Langley, 1968 —— 1 A-2808

"The aeronautical and space activities of the United States shall be conducted so as to contribute . . . to the expansion of human knowledge of phenomena in the atmosphere and space. The Administration shall provide for the widest practicable and appropriate dissemination of information concerning its activities and the results thereof."

—NATIONAL AERONAUTICS AND SPACE ACT OF 1958

NASA SCIENTIFIC AND TECHNICAL PUBLICATIONS

TECHNICAL REPORTS: Scientific and technical information considered important, complete, and a lasting contribution to existing knowledge.

TECHNICAL NOTES: Information less broad in scope but nevertheless of importance as a contribution to existing knowledge.

TECHNICAL MEMORANDUMS: Information receiving limited distribution because of preliminary data, security classification, or other reasons.

CONTRACTOR REPORTS: Scientific and technical information generated under a NASA contract or grant and considered an important contribution to existing knowledge.

TECHNICAL TRANSLATIONS: Information published in a foreign language considered to merit NASA distribution in English.

SPECIAL PUBLICATIONS: Information derived from or of value to NASA activities. Publications include conference proceedings, monographs, data compilations, handbooks, sourcebooks, and special bibliographies.

TECHNOLOGY UTILIZATION PUBLICATIONS: Information on technology used by NASA that may be of particular interest in commercial and other non-aerospace applications. Publications include Tech Briefs, Technology Utilization Reports and Notes, and Technology Surveys.

Details on the availability of these publications may be obtained from:

SCIENTIFIC AND TECHNICAL INFORMATION DIVISION

NATIONAL AERONAUTICS AND SPACE ADMINISTRATION

Washington, D.C. 20546